Journal of Crystal Growth 312 (2010) 1957–1962

Contents lists available at ScienceDirect

Journal of Crystal Growth

journal homepage: www.elsevier.com/locate/jcrysgro

Synthesis, growth, structural, thermal, linear and nonlinear optical properties of a new organic crystal: Dimethylammonium picrate

G. Anandha Babu [a,*], S. Sreedhar [b], S. Venugopal Rao [b], P. Ramasamy [a]

[a] Centre for Crystal Growth, SSN College of Engineering, SSN Nagar, Tamilnadu 603 110, India
[b] Advanced Centre of Research in High Energy Materials, University of Hyderabad, Hyderabad 500 046, India

ARTICLE INFO

Article history:
Received 5 January 2010
Received in revised form
23 February 2010
Accepted 15 March 2010
Communicated by M. Schieber
Available online 30 March 2010

Keywords:
A1. X-ray diffraction
A2. Growth from solutions
B1. Organic compounds
B2. Nonlinear optic materials

ABSTRACT

Single crystal of dimethylammonium picrate (DMAP) was successfully grown for the first time by the slow evaporation method with dimensions $25 \times 15 \times 10\ mm^3$. ^1H NMR was recorded to elucidate the molecular structure. The cell parameters were determined from single crystal X-ray diffraction studies. The crystal has eight developed facets with major ones (0 0 1) and (0 0 −1). The structural perfection of the grown crystals has been analyzed by high-resolution X-ray diffraction (HRXRD) rocking curve measurements. Fourier transform infrared (FTIR) spectral studies have been performed to identify the functional groups. Thermo gravimetric analysis (TGA) and differential thermal analysis (DTA) were used to study its thermal properties. Powder test with Nd:YAG laser radiation shows second harmonic generation. The proton donor (–OH) group and proton acceptor amine (–NH) group in the DMAP structure provide infrastructure to introduce the charge asymmetry. The optical transmittance window and the lower cutoff wavelength of the DMAP have been identified by UV–vis–NIR studies. The laser induced surface damage threshold for the grown crystal was measured using Nd:YAG laser. The dielectric properties of DMAP from 323 to 373 K were investigated by the impedance analysis. The microhardness test was carried out and the load dependent hardness was measured.

1. Introduction

In recent years, an intense worldwide effort has been focused on the design and development of highly efficient organic nonlinear optical (NLO) materials [1]. The nonlinearity of organic compounds having a π-electron conjugated system is caused by nonlinear polarization that occurs due to the interaction between laser light which comprises a strong electromagnetic wave and the delocalized π-electrons in the organic molecule of interest. In order to increase the magnitude of nonlinear polarization of the molecule, an electron donating group (donor) or an electron withdrawing group (acceptor) is introduced into the π-electron conjugated system as a common technique for molecular design. Organic nonlinear materials have the advantage that they are less costly and can be synthesized fairly easily. However, the absorption wavelength range of such organic materials, if they have a high SHG efficiency, extends to visible region and their crystals show a yellow or orange color, which makes them useless to wavelength conversion of semiconductor lasers. Finding ways to ensure that a bulk material is acentric has been a serious hurdle in the design of new organic materials for NLO uses. Various strategies have been proposed to get noncentrosymmetric packing. These include chirality, hydrogen bonding [2], reduced dipole–dipole interaction [3], etc. The proton transfer between two separate NLO organic compounds takes place and results in a noncentrosymmetric organic salt, then this could increase the hyperpolarizability of both species, provided one is an acid and the second is a base. The first purposeful utilization of this strategy (proton transfer) to increase the hyperpolarizabilities of the organic compounds was proposed. Picric acid derivatives are interesting candidates, as the presence of phenolic OH favors the formation of salts with various organic bases. The conjugated base, picrate, thus formed has increased molecular hyperpolarizability because of the proton transfer. On the basis of this, in the present investigation we report for the first time, the growth, crystal morphology, structural, electrical, thermal, laser damage threshold, linear and NLO studies of the title compound dimethylammonium picrate.

2. Experimental procedures

2.1. Material synthesis

The title compound was synthesized by reacting equimolar quantities of dimethylamine and picric acid in acetone. When a

* Corresponding author. Tel./fax: +91 4427475166.
E-mail address: anandcgc@gmail.com (G. Anandha Babu).

0022-0248/$ - see front matter © 2010 Elsevier B.V. All rights reserved.
doi:10.1016/j.jcrysgro.2010.03.017

proton is transferred from the electron-donor group of an acid to the electron acceptor group of a base it results in increase of hyperpolarizability of the resultant compound. Fig. 1 represents the reaction scheme for the formation of the title compound. The picric acid OH group necessarily protonates the nitrogen of the dimethylamine resulting in the formation of the title compound.

2.2. Solubility and crystal growth

To realize the practical applications, good quality single crystals of reasonable size are essential. The material was purified from acetone solution by the recrystallization process. The solubility of DMAP in acetone was assessed as a function of temperature in the range 25–35 °C. The DMAP exhibits good solubility and a positive solubility-temperature gradient in acetone. Fig. 2 shows the solubility curve for DMAP. Single crystal of size $25\times15\times10\,mm^3$ has been obtained after a typical period of 10 days. Grown single crystal of DMAP is shown in Fig. 3.

The grown crystals were subjected to X-ray diffraction studies using Nonius CAD4/MACH 3 single crystal X-ray difffractometer, using MoK$_\alpha$ (λ=0.71073 Å). The crystalline perfection of the DMAP single crystals grown by slow evaporation solution growth technique (SEST) was characterized by HRXRD by employing a multicrystal X-ray diffractometer developed at National Physical Laboratory, New Delhi. The well-collimated and monochromated MoKα_1 beam obtained from the three monochromator Si crystals set in dispersive (+,−,−) configuration has been used as the exploring X-ray beam. The specimen crystal is aligned in the (+,−,−,+) configuration. Due to dispersive configuration, though the lattice constants of the monochromator crystal(s) and the specimen are different, the unwanted dispersion broadening in the diffraction curve (DC) of the specimen crystal is insignificant. The specimen can be rotated about the vertical axis, which is perpendicular to the plane of diffraction, with minimum angular

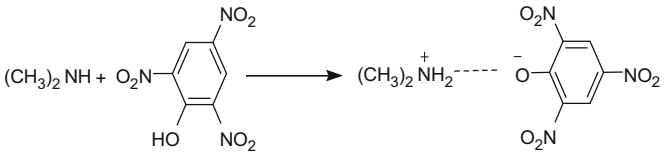

Fig. 1. Reaction scheme for DMAP.

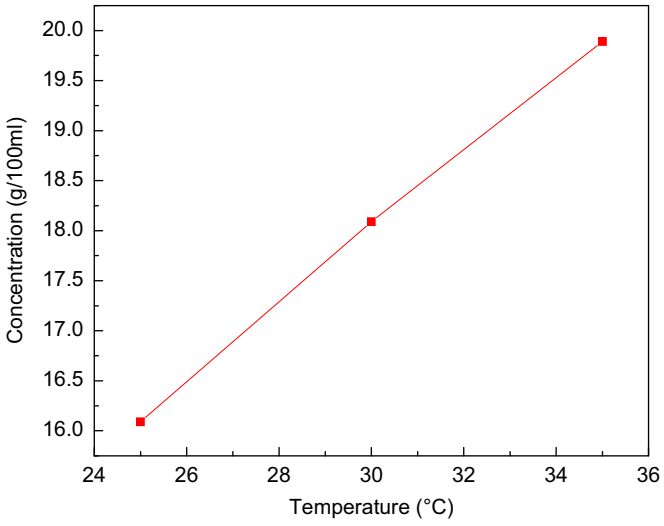

Fig. 2. Solubility curve of DMAP in acetone.

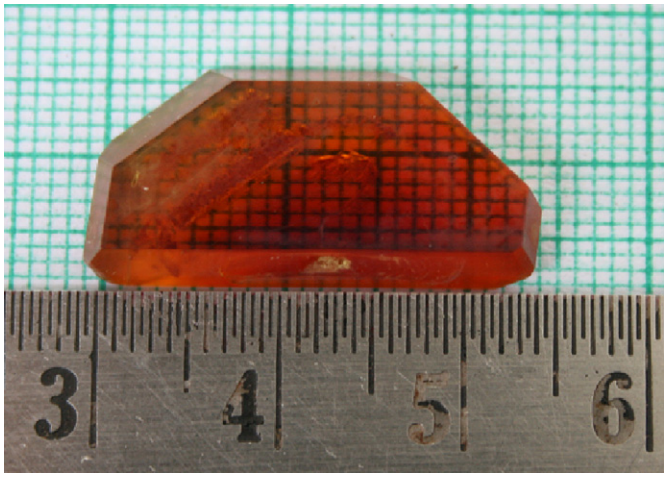

Fig. 3. Grown single crystal of DMAP.

interval of 0.4 arcsec. The DC was recorded by the so-called ω scan wherein the detector was kept at the same angular position $2\theta_B$ with wide opening for its slit. Before recording the diffraction curve to remove the non-crystallized solute atoms which remained on the surface of the crystal and also to ensure the surface planarity, the specimen was first lapped and chemically etched in a non preferential etchant of water and acetone mixture in 1:2 volume ratio. The ^{1}H NMR spectrum of the sample was recorded using an AMX 400 MHz spectrometer in DMSO-d$_6$ solvent using tetramethyl silane as the internal reference standard. FTIR spectrum was recorded from potassium bromide pellets on a Perkin Elmer FTIR spectrometer in the range 4000–450 cm^{-1}. The transmission spectrum of the DMAP crystal was studied in the range 200–1100 nm by Perkin Elmer spectrometer. Transparent single crystal of 1 mm thickness was used for this study. The TGA and DTA experiments were carried out on a NETZSCH STA 409 instrument with a heating rate of 10 °C/min from 30 to 800 °C. Samples were weighed in an Al_2O_3 crucible. Quantitative measurement of relative efficiency of DMAP with respect to KDP was made by the Kurtz and Perry powder technique. The finely powdered crystal of DMAP was packed in capillary tube. An Nd:YAG laser (DCR11) was used as a light source. A laser beam of fundamental wavelength 1064 nm, 8 ns pulse width, with 10 Hz pulse rate was made to fall normally on the sample cell. The power of the incident beam was measured using a power meter. The transmitted fundamental wave was passed over a monochromator (Czemy Turner monochromator), which separates 532 nm (second harmonic signal) from 1064 nm, and absorbed by a $CuSO_4$ solution, which removes the 1064 nm light, and passed through BG-34 filter to remove the residual 1064 nm light and an interference filter with bandwidth of 4 nm and central wavelength of 532 nm.

A Q-switched Nd:YAG (yttrium aluminum garnet) Innolas laser of pulse width 7 ns and 10 Hz repetition rate operating in TEM$_{00}$ mode is used as the source. The energy per pulse of 532 nm laser radiation attenuated using high energy variable attenuator is measured using an energy power meter (Scientech Inc.) which is externally triggered by the Nd:YAG laser. Since the surface damage is affected by the energy absorbing defects such as polishing contaminants and surface scratches, which get incorporated during mechanical polishing, all the experiments are performed on the highly polished crystals (uniformly polished with high quality polishing powder) thus minimising the strain and incorporation of impurities. For both single and multiple shot experiments, the sample is mounted on an X–Y translator that facilitates in bringing different areas of the sample for exposure

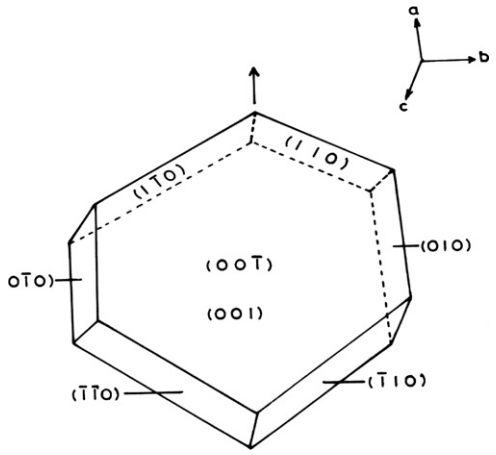

Fig. 4. Morphology of DMAP crystal.

precisely. For surface damage, the sample is placed at the focus of a plano-convex lens of focal length 80 mm. The onset of damage can be determined by visual damage and audible cracking.

The capacitance (C_{crys}) and dielectric loss ($\tan\delta$) were measured using the conventional parallel plate capacitor method with frequency range (1 KHz to 1 MHz) using Agilent 4284 A LCR meter at various temperatures ranging from 323 to 373 K. Vickers microhardness measurement studies were also carried out using a Leitz–Wetzlar hardness tester. Loads ranging from 35 to 140 g were used for making indentations, keeping the time of indentation constant at 20 s for all the cases.

3. Results and discussions

It was observed that the growth rate of DMAP along the *a*- and *b*-axes is much higher than that along the *c*-axis. As depicted in Fig. 4, the morphology is a polyhedron with eight symmetrically independent facets. Among these facets, the crystal has two prominent flat facets. For each face, its parallel Friedel plane is also present in the grown crystal and shown diagrammatically in Fig. 4.

The recorded ^{1}H NMR spectrum is shown in Fig. 5. The spectrum exhibits three proton signals confirming the presence of the different kinds of protons in the crystal. The intense proton signal appearing at $\delta=8.60$ ppm is due to the two aromatic protons of the kind in the picrate moiety of the crystal. A small hump at $\delta=8.17$ ppm is attributed to the two amino protons in the dimethylaminium moiety. The six chemically and magnetically equivalent methyl protons stand responsible for the intense signal at $\delta=2.55$ ppm. Thus the molecular structure stands confirmed from the ^{1}H NMR spectral data.

From the single crystal X-ray diffraction studies, it is observed that the crystal belongs to the orthorhombic system with the space group of $Pca2_1$ and the unit cell parameters are $a=9.995(3)$ Å, $b=11.119(8)$ Å, $c=21.326(7)$ Å and $\alpha=\beta=\gamma=90^\circ$. The crystal structure was already reported by Walkinshaw [4].

Fig. 6 shows the high-resolution diffraction curve (DC) recorded for DMAP specimen using (2 2 0) diffracting planes in symmetrical Bragg geometry by employing the multicrystal X-ray diffractometer described above with MoKα_1 radiation. As seen in Fig. 6, the DC is quite sharp without any satellite peaks which may otherwise be observed either due to internal structural grain boundaries [5] or due to epitaxial layer which may sometimes form in crystals grown from solution [6]. The full width at half maximum (FWHM) of the diffraction curves is 15 arcsec, which is close to that expected from the plane wave theory of dynamical

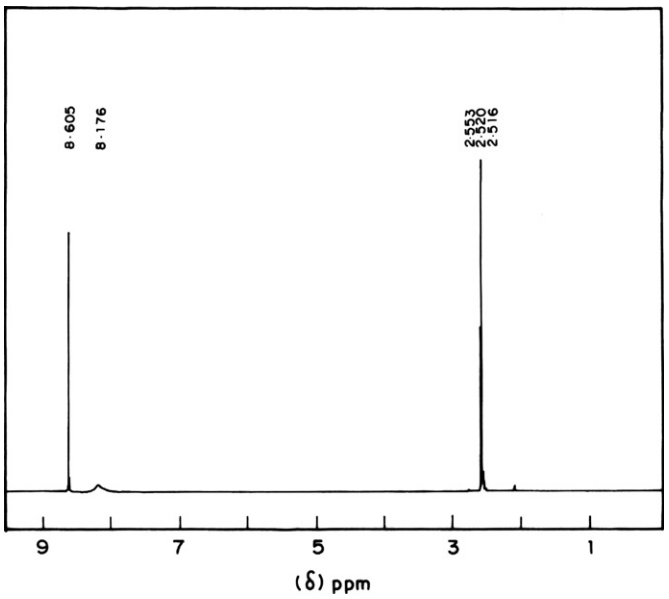

Fig. 5. ^{1}H NMR spectrum of DMAP.

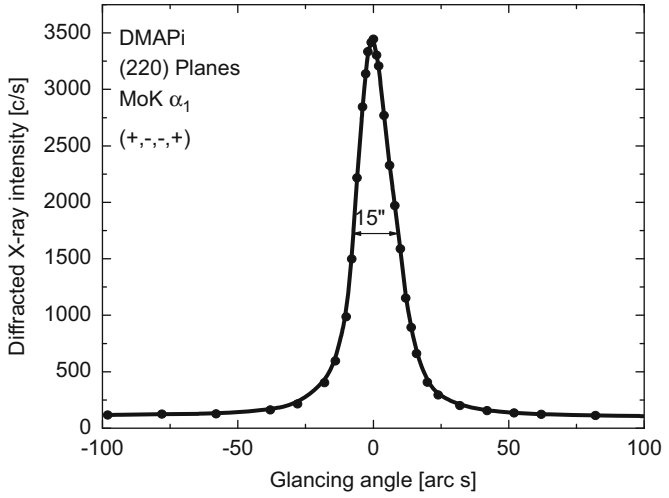

Fig. 6. Diffraction curve recorded for a typical DMAP single crystal for (0 2 0) diffracting planes by employing the multicrystal X-ray diffractometer with MoKα_1 radiation.

X-ray diffraction [7]. The single sharp diffraction curve with low FWHM indicates that the crystalline perfection is very good. The specimen is a nearly perfect single crystal without having any internal structural grain boundaries.

The recorded infrared spectrum is shown in Fig. 7. In the FTIR spectrum of DMAP, the $-NO_2$ asymmetric stretching vibration appears at 1544 cm^{-1}. The corresponding symmetric stretching vibrations occur at 1333 cm^{-1}. The $-NO_2$ scissoring vibrational modes appear in the spectra of DMAP at 890 cm^{-1}. The NO_2 rocking vibration is observed at 547 cm^{-1}. The aromatic C–H in-plane bending vibration occurs at 1167 cm^{-1}. The aromatic C–H out of plane vibration occurs at 911 cm^{-1}. The band at 1549 cm^{-1} is due to the O–H in-plane deformation mode. The asymmetric N^+–H deformation mode occurs at 1610 cm^{-1}. The asymmetric and symmetric stretching vibrations of methyl groups in DMAP appear, respectively, at 3090 and 2840 cm^{-1}. The C–H asymmetric and symmetric deformation modes of methyl groups appear at 1489 and 1363 cm^{-1}, respectively. The C–O

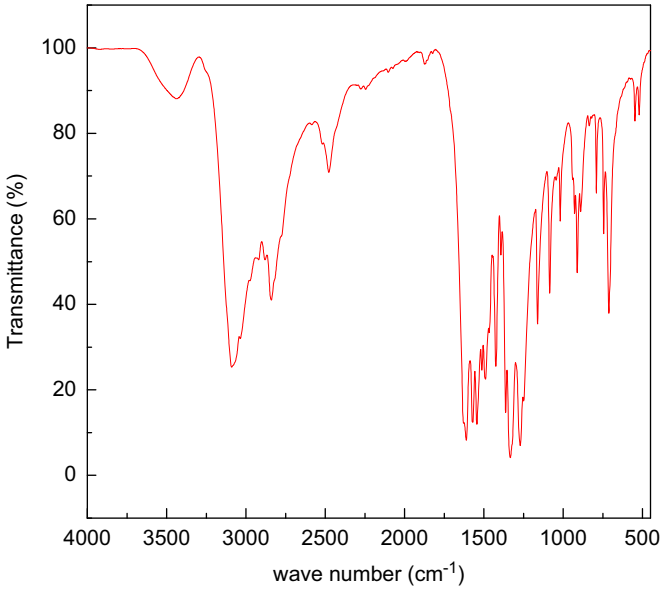

Fig. 7. FTIR spectrum of DMAP.

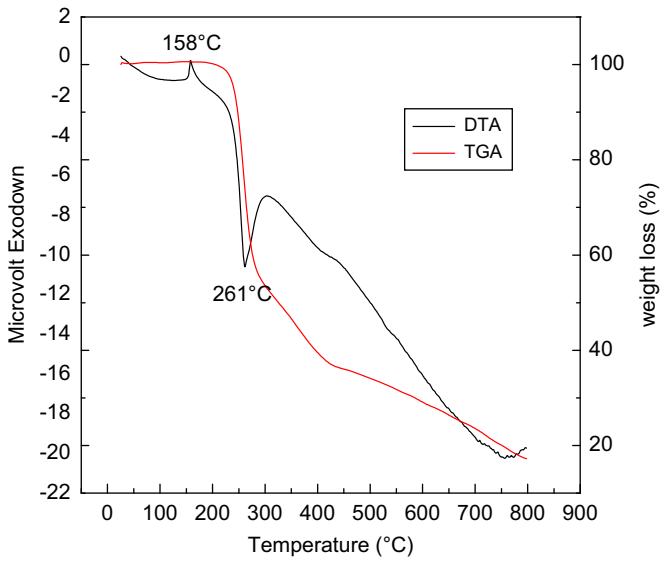

Fig. 9. TG-DTA curves of DMAP.

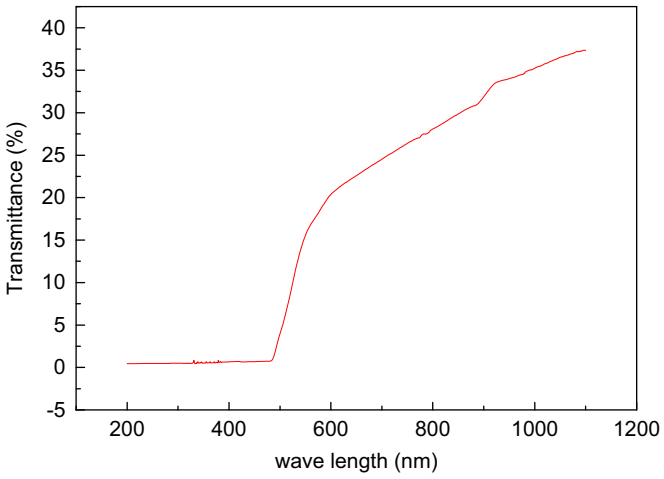

Fig. 8. UV–vis–NIR spectrum of DMAP.

stretching appears at 1271 cm^{-1}. In aromatic nitro compounds the C–NO_2 stretching vibration occurs at 928 cm^{-1}.

The UV–vis–NIR spectrum of DMAP is shown in Fig. 8. The transmission range and transparency cutoff are very important parameters, especially for crystals used in SHG. DMAP crystal presents a cutoff wavelength at 500 nm. It means that DMAP crystal might be used for SHG for a 1064 nm laser if DMAP can fit phase matching conditions. Molecular NLO crystals usually have high absorption in the visible wavelength region and a narrow transparency window. This is one of the disadvantages of molecular NLO crystals. The high excited-to-ground state dipole moment that increases the nonlinearity also increases absorption. The low percentage of transmission can be attributed to the purity of the starting material, growth method and surface polishing.

The thermal behavior of DMAP has been identified from the TG/DTA. Fig. 9 shows the thermal properties of the DMAP crystal carried out by TGA and DTA. In the differential thermogram, sharp endothermic peak was found at 158 °C. The endothermic is assigned to the melting point at which no weight loss in TG has been noticed. The sharp exothermic reaction around 261 °C may be possibly due to some complex formation. There is steep loss of weight starting around 261 °C and after complex formation the weight loss is relatively gradual. The final residue weight left was about 20% after heating to 800 °C. The DMAP material has fairly high melting point.

The dielectric properties are correlated with the electric field distribution within crystal. The prominent (0 0 1) plane was polished using fine-grade alumina powder. Figs. 10(a) and (b) show variation of dielectric constant and dielectric loss dependence of frequency at 100 °C. The dielectric constant is relatively high in the lower frequency and becomes almost saturated beyond 100 KHz. This may be due to the interfacial polarization, in which the mobile charge carriers are interdicted by a physical barrier which retains genernating a localized polarization of the material. The higher values of dielectric loss at low frequencies originate from space charge polarization mechanism dipoles, and the characteristic of low dielectric loss at high frequencies clarifies that the grown samples possess enhanced optical quality with lesser defects [8,9].

The plot of dielectric constant as a function of various temperatures at different frequencies is given in Fig. 10(c). It is obvious that the variation of dielectric constant with temperature is small, which infers that the crystals are of good chemical homogeneity [10].

Powder test with Nd:YAG laser radiation shows second harmonic generation. The proton donor (–OH) group and proton acceptor amine (–NH) group in the structure provide infrastructure to introduce the charge asymmetry formed. This charge asymmetry is required for second order nonlinearity. The beam energy with 1.58 mJ/pulse was used. The SHG signal energy outputs are 95 and 192 mV for KDP and DMAP sample, respectively. This strongly suggests the title compound as a potential candidate for SHG applications. The SHG value of some picrate NLO crystals (compared to KDP) is given in Table 1 for the purpose of comparsion. Compared to other picrate crystals DMAP grows as a good bulk crystal with well-developed facets thus enabling easier preparation of SHG element.

The operation of nonlinear devices obviously involves the exposure of material to high power laser source. For harmonic generation, the efficiency of conversion is strongly dependent on the incident power level. The utility of NLO crystal depends not only on the linear and nonlinear optical properties but also largely on its ability to withstand high power lasers. The bulk materials

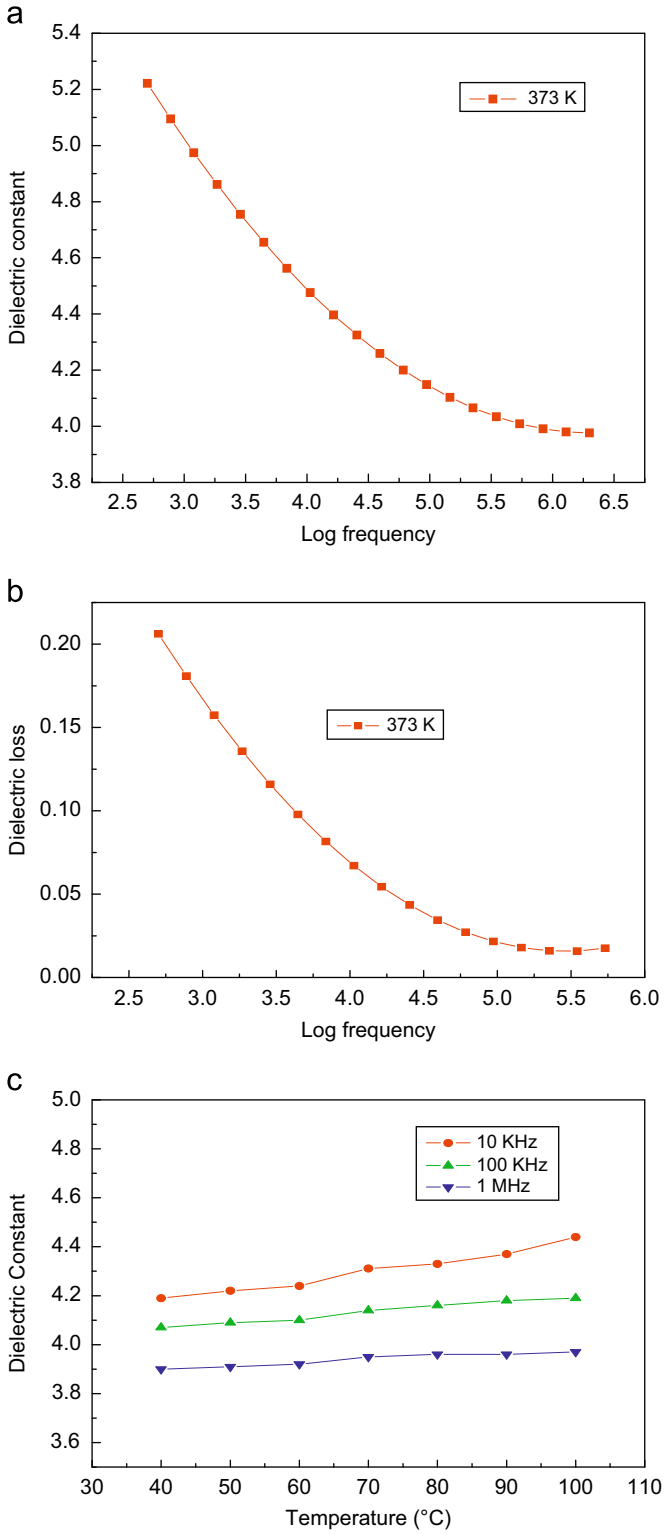

Fig. 10. Variation of dielectric constant (a) and dielectric loss (b) of DMAP with log frequency at 373 K, respectively; (c) variation of dielectric constant of DMAP with temperature.

appear more damage-resistant than the surfaces. Therefore, the performance of the crystal mainly depends on surface quality [14]. In fact, the polishing process used in the finishing of optical elements leaves residual scratches and imperfections on the surface. At these points, the electric field in the light wave is greatly intensified so that the effective field value just inside the

Table 1
Properties of some picrate nonlinear optical crystals.

Name	Powder SHG (X KDP)	Melting point (°C)	Reference
LPP	52	250	[11]
LVAP	144	170	[12]
LASP	67	–	[13]
DMAP	2	158	Present work

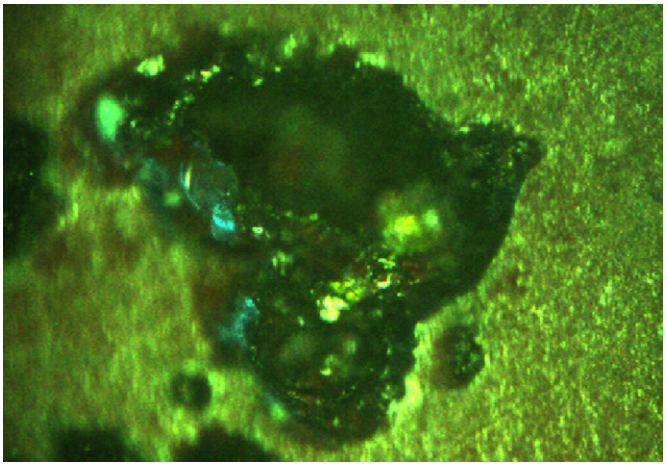

Fig. 11. Laser damage profile of DMAP.

surface is much greater than the average field. When break-down or failure of the surface occurs, it occurs near one of these imperfections. Furthermore, damage also occurs due to minute inclusions of polishing materials, airborne particles, finger prints, etc., providing a nucleus around which damage may occur. Thus, the surface damage is caused either by absorption of sub-micron inclusions or by formation of a plasma at the surface because of electron avalanche breakdown in the dielectric. However, the local heating caused by macroscopic inclusion is a more severe problem in high intensity short-pulse system than in low-intensity long-pulse or cw system of equal average intensity. Moreover, the occurrence of damage is probabilistic in its nature, and the laser pulse whose power is lower than the single-shot damage threshold still has a non-zero probability to cause damage [15]. However, damage threshold depends on a great number of laser parameters such as wavelength, energy, pulse duration, transverse and longitudinal mode structure, beam size, location of beam, etc. The diameter of the focused spot is calculated to be 1.08 mm using knife edge method.

The surface damage threshold of the crystals was calculated using the expression

$$\text{Powerdensity } (P_d) = \frac{E}{\tau \pi r^2}$$

where E is the energy (mJ), τ the pulse width (ns) and r the radius of the spot (mm). Single shot and multiple shot (20 pulses) surface laser damage thresholds are determined to be 0.34 and 0.26 GW/cm^2, respectively, at 532 nm laser radiation.

Fig. 11 shows the optical micrograph of the single shot damage profile of 532 nm laser radiation of DMAP. The mechanism of laser induced damage in materials is often very complex involving various processes like electron avalanche, multi-photon absorption, photo-ionization by thermal absorption [16], photo-chemical dissociation [17], electrostrictive fracture, etc. Exactly which one dominates depends on factors like the specific

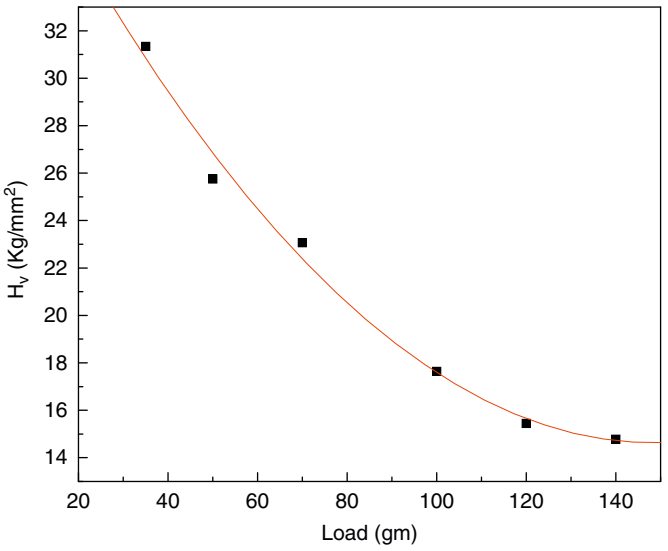

Fig. 12. Plot of Vickers hardness number versus load.

properties of the material under investigation, experimental geometry, wavelength and pulse width of the laser radiation used. From an earlier report [18], it is known that in the long-pulse regime ($\tau > 100$ ps), the damage is controlled by the rate of thermal conduction through the atomic lattice and in the short-pulse regime ($\tau < 100$ ps), the optical breakdown and various nonlinear ionization mechanisms (multi-photon, avalanche multiplication, tunneling) become important. Hence, thermal effects become important for the pulse widths that are nanoseconds and longer and in the case of picosecond and femtosecond pulse widths for higher repetition rates wherein the cumulative effects become prominent. It may be noted that in the present case we have used 7 ns pulse. In most of the cases a careful examination of the damage pattern gives some idea about the underlying mechanism of the laser induced damage [19]. The damage pattern of DMAP (Fig. 11) shows tiny circular blobs surrounding the core of the damage. Such circular blobs are generally seen in crystals where the damage is mainly due to thermal effects resulting in melting and solidification or decomposition of the material [20]. Recent investigations into laser damage in various optical materials by nanosecond pulses have shown that the temperature reached at the damage site could be as high as 12,000 K [21]. Since DMAP decomposes at around 220 °C it is most likely that in the present case damage occurs due to decomposition of the crystal. Hence, in DMAP we can expect the damage to be of thermal origin. However, one cannot rule out other mechanisms being operative simultaneously, as the damage mechanism is quite complex and depends on the nature of the material and various experimental parameters.

The mechanical properties of crystalline materials are closely related with their other physical properties, and determine the performance of devices prepared from the solids. Fig. 12 shows the variation of H_v as a function of applied load ranging from 35 to 140 g for the DMAP crystal. It is very clear from the figure that H_v decreases with the increase of load. It is well known that the microhardness of solids depends on the applied indentation test load. This phenomenon, known as the indentation size effect, usually involves a decrease in the Vickers microhardness with increasing applied test load.

4. Conclusion

Optical quality single crystals of DMAP were grown using solution growth technique. The unit-cell parameters of DMAP were confirmed by single crystal X-ray diffraction analysis. The high-resolution X-ray diffraction curve (DC) measurements substantiate the good quality of the crystals. The functional group was confirmed by FTIR. In the transmittance spectra, it is evident that the DMAP crystal has a fairly wide transparency range. The thermal behavior of the grown crystals was studied by using TG-DTA. Powder test with Nd:YAG laser radiation shows second harmonic generation. Thus, DMAP seems to be a promising material for NLO application. Single shot and multiple shot (300 pulses) surface laser damage thresholds are determined to be 0.34 and 0.26 GW/cm^2 at 532 nm laser radiation, respectively. Thermal breakdown is identified as the plausible mechanism for laser induced damage in this crystal.

Acknowledgments

The authors thank Prof. P.K. Das, Indian Institute of Science, Bangalore, for support in SHG measurement. We thank Dr. G. Bhagavannarayana, National Physical Laboratory, New Delhi for HRXRD studies.

References

[1] X.J. Liu, Z.Y. Wang, X.Q. Wang, G.H. Zhang, S.X. Xu, A.D. Duan, S.J. Zhang, Z.H. Sun, D. Xu, Cryst. Growth Des. 8 (2008) 2270–2274.
[2] J. Zyss, I. Ledoux, R.B. Hierle, R.K. Raj, J.L. Oudar, IEEE J. Quantum Electron. 21 (1985) 1286–1295.
[3] J. Zyss, D.S. Chemla, I.F. Nicoud, J. Chem. Phys. 74 (1981) 4800.
[4] M.D. Walkinshaw, Acta Cryst. C C42 (1986) 246–249.
[5] G. Bhagavannarayana, R.V. Ananthamurthy, G.C. Budakoti, B. Kumar, S. Bartwal, J. Appl. Cryst. 38 (2005) 768–771.
[6] G. Bhagavannarayana, S. Parthiban, Subbiah Meenakshisundaram, J. Appl. Cryst. 39 (2006) 784–790.
[7] B.W. Betterman, H. Cole, Rev. Mod. Phys. 36 (1964) 681–717.
[8] C.P. Smyth, in: Dielectric Behaviour and Structure, McGraw Hill, New York, 1995 132.
[9] C. Balarew, R. Duhlew, J. Solid-State Chem. 55 (1984) 1.
[10] V.A. Hiremath, A. Venkataraman, Bull. Mater. Sci. 26 (2003) 391.
[11] T. Uma Devi, N. Lawrence, R. Ramesh Babu, K. Ramamurthi, J. Cryst. Growth 310 (2008) 116–123.
[12] P. Srinivasan, T. Kanagasekaran, R. Gopalakrishnan, Cryst. Growth Des. 8 (2008) 2340–2345.
[13] P. Srinivasan, T. Kanagasekaran, R. Gopalakrishnan, G. Bhagavannarayana, P. Ramasamy, Cryst. Growth Des. 6 (2006) 1663–1670.
[14] N.L. Boling, M.D. Crisp, G. Dube, Appl. Opt. 12 (1973) 650–660.
[15] M. Bass, H.H. Barrett, Appl. Opt. 12 (1973) 690–699.
[16] A.J. Glass, A.H. Guenther, Appl. Opt. 12 (1973) 637–649.
[17] R.T. Bailey, F.R. Cruickshank, P. Kerkoc, D. Pugh, J.N. Sherwood, Appl. Opt. 34 (1995) 1239–1244.
[18] B.C. Stuart, M.D. Feit, A.M. Rubenchik, B.W. Shore, M.D. Perry, Phys. Rev. Lett. 74 (1995) 2248–2251.
[19] M. Yoshimura, T. Kamimura, K. Murase, Y. Mori, H. Yoshida, M. Nakatsuka, T. Sasaki, Jpn. J. Appl. Phys. 38 (1999) L129–L131.
[20] A.J. Glass, A.H. Guenther, Appl. Opt. 12 (1973) 637–649.
[21] C.W. Carr, H.B. Radousky, A.M. Rubenchik, M.D. Feit, S.G. Demos, Phys. Rev.Lett. 92 (2004) 087401–087403.